Journal of Nuclear Medicine, published on October 27, 2016 as doi:10.2967/jnumed.116.178103

Preclinical Evaluation and Quantification of ^{18}F-Fluoroethyl and ^{18}F-Fluoropropyl analogs of SCH442416 as Radioligands for PET Imaging of the Adenosine A_{2A} Receptors in Rat Brain

Shivashankar Khanapur[1], Aren van Waarde[1], Rudi A.J.O. Dierckx[1], Philip H. Elsinga[1], Michel J.B. Koole[1,2]

[1]Department of Nuclear Medicine and Molecular Imaging, University of Groningen, University Medical Center Groningen, Groningen, The Netherlands

[2]Department of Nuclear Medicine and Molecular Imaging, KU Leuven, Leuven, Belgium

Corresponding author: Michel Koole, PhD, KU Leuven, Division of Nuclear Medicine, Herestraat 49, 3000 Leuven, Belgium, Telephone + 32 16 341242, Telefax +32 16 343759, E-mail: michel.koole@kuleuven.be (associate professor)

First Author: Dr. Shivashankar Khanapur, PhD, University of Groningen, University Medical Center Groningen, Nuclear Medicine and Molecular Imaging, Hanzeplein 1, 9713GZ Groningen, The Netherlands, Telephone +31-50-3613375, Telefax +31-50-3611687, E-mail: shivakhanapur4u@gmail.com (post-doctoral research fellow)

Word count: 5126

Short Running title: Quantifying ^{18}F-SCH442416 analogs

ABSTRACT

Cerebral adenosine A_{2A} receptors (A_{2A}Rs) are attractive therapeutic targets for neuropsychiatric disorders. ^{18}F-Fluoroethyl and ^{18}F-fluoropropyl analogs of SCH442416 (^{18}F-FESCH and ^{18}F-FPSCH) were developed as A_{2A}R specific PET ligands. Aim is to determine an appropriate compartmental model for tracer kinetics, evaluate a reference tissue approach and select the most suitable PET ligand. **Methods:** A 90 min dynamic PET with arterial blood sampling and metabolite analysis was acquired for 22 healthy male Wistar rats starting at ^{18}F-FESCH (n = 12) and ^{18}F-FPSCH (n = 10) injection. For each tracer, half of the number of animals was vehicle-treated while the other half was pretreated with the A_{2A}R-selective antagonist KW-6002, inducing full blocking. Regional tissue distribution volumes (V_T) were estimated by 1- and 2-tissue compartment modeling (TCM) and Logan graphical analysis. Midbrain, cerebellum and hippocampus were evaluated as reference region by comparing baseline V_T with V_T under full blocking conditions and comparing striatal BP_{ND} (Binding Potential) using a Simplified Reference Tissue Model (SRTM) with DVR-1 (Distribution Volume Ratio) for a 60 and 90 min scan duration. **Results:** Based on Akaike Information Criterion (AIC), 1TCM and 2TCM were the most appropriate models for ^{18}F-FPSCH (baseline striatal $V_T = 3.7 \pm 1.1$) and ^{18}F-FESCH (baseline striatal $V_T = 5.0 \pm 2.0$) respectively. Baseline striatal V_T was not significantly different between both tracers. After pretreatment, striatal V_T was reduced significantly with no significant decrease of hippocampus, midbrain and cerebellum V_T. Baseline striatal SRTM BP_{ND} did not differ significantly from DVR-1 except for ^{18}F-FPSCH when using a 60 min scan and midbrain as reference region while a Bland Altman analysis found a smaller bias for ^{18}F-FESCH and a 60 min scan. After pretreatment, striatal SRTM BP_{ND} values were not significantly different from zero except for ^{18}F-FPSCH when using hippocampus as reference region. Striatal SRTM BP_{ND} using midbrain or cerebellum as reference region was significantly lower for ^{18}F-FPSCH (range: 1.41 - 2.62) compared to ^{18}F-FESCH (range: 1.64 - 3.36). **Conclusion:** Dynamic PET imaging under baseline and blocking conditions determined ^{18}F-FESCH as the most suitable PET ligand for quantifying A_{2A}R expression in the rat brain. Accurate quantification is achieved by a 60 min dynamic PET scan and using either cerebellum or midbrain as reference region.

Keywords: Preclinical Positron Emission Tomography (μPET), cerebral adenosine A_{2A} receptors, ^{18}F-SCH442416 analogs, Kinetic Analysis, Rat Brain.

INTRODUCTION

Adenosine, an extracellular endogenous signaling molecule, is released to either reduce the energy demand or increase the energy supply to an organ or tissue which is damaged or stressed, and thereby elicits cytoprotective and neuromodulatory effects via four different G-protein coupled adenosine receptors (ARs) ; A_1, A_{2A}, A_{2B}, and A_3 (*1-5*). Out of these ARs, high affinity adenosine A_1 and A_{2A}Rs have been extensively studied because these are well-characterized both pharmacologically and biochemically *(6)*. Within the human brain, A_1Rs are ubiquitously present but high expression levels occur in the hippocampus, cerebral cortex, thalamic nuclei, and dorsal horn of spinal cord whereas A_{2A}Rs are restricted to the basal ganglia and particularly abundant in the striatum. Lower levels of A_{2A}Rs are expressed in several brain regions including hippocampus, cerebral cortex, amygdala, cerebellum, brainstem and hypothalamus *(7-10)*.

Many studies have reported a dysregulation of A_{2A}Rs in neuropsychiatric disorders such as Parkinson's, Huntington's and Alzheimer's diseases, attention deficit hyperactivity and panic disorders, schizophrenia, pain and impaired sleep *(11)*. A number of studies suggested that A_{2A}Rs may play an important role in the regulation of dopaminergic and glutamatergic neurotransmission in the basal ganglia through antagonistic interactions with dopamine D_2 receptors and by forming functional heterodimers with metabotropic glutamate receptor 5, cannabinoid receptor type 1, and adenosine A_1Rs *(12-14)*. Positron emission tomography (PET) with high affinity and selective A_{2A}R antagonist radioligands can be used to exploit changes in A_{2A}Rs distribution and density during disease progression and to monitor treatment response on such changes. Furthermore, PET can be employed to assess A_{2A}R occupancy by investigational drugs in the human brain, thereby providing a useful tool for the drug discovery process *(11)*.

Several PET radiotracers have been developed and evaluated for in vivo imaging of A_{2A}Rs in the brain (*15-23*). We have developed ^{18}F-FESCH and ^{18}F-FPSCH analogs (Fig. 1) and evaluated them in healthy rats *(6)*. Preliminary evaluation of these tracers showed a distribution corresponding to the known regional A_{2A}R densities in the rat brain. Moreover, both tracers demonstrated slightly different but reversible kinetics with a lower nonspecific binding and a higher striatum-to-cerebellum ratio compared to ^{11}C-SCH442416. Metabolite analyses indicated the presence of hydrophilic (radio)metabolite(s), which are not expected to cross the blood-brain barrier *(6)*.

The aim of the present study was to develop a suitable tracer kinetic model for the quantification of cerebral A_{2A}Rs with these radiofluorinated A_{2A}R ligands and to evaluate a reference tissue approach. In addition, it also reports the possible reduction in acquisition time. Based on these findings, we will select the most suitable PET ligand for further preclinical use.

MATERIALS AND METHODS

General materials and Radiosyntheses are presented in supplemental materials (available at http://jnm.snmjournals.org). The synthesis, radiolabeling and quality control of ^{18}F-FESCH and ^{18}F-FPSCH was described in detail previously *(6)*.

Small-animal PET scanning

The animal experiments were carried out by licensed investigators in compliance with the law on Animal experiments of The Netherlands. The institutional Animal care and use committee of the University of Groningen approved the protocols. A total of 22 male outbred Wistar-Unilever rats was included in the study design, subdivided into a control and pretreatment group for each tracer (Table 1). Five minutes prior to *i.v.* tracer administration, animals of the pretreated group were administered a cold A_{2A}R antagonist, KW-6002 (1 mg / kg, 50 % dimethylacetamide : saline (v / v)), by intraperitoneal injection (i.p.) in order to prove saturability and specific binding of the tracers in the brain (*18*,*24*). Since ED_{50} of KW-6002 in rat striatum for i.p. injection was 0.044–0.062 mg / kg, as was demonstrated by a dose occupancy study with ^{11}C-preladenant, administration of 1 mg / kg of KW-6002 by i.p. injection is expected to fully block the A_{2A}R receptors in rat brain (*23*). Volume of the vehicle (solvent) was 1 mL / kg corresponding to a volume of 0.3 mL for an average rat with a weight of 300 g. For each animal a dynamic PET scan was acquired and reconstructed with 8 × 30, 3 × 60, 2 × 120, 2 × 180, 3 × 300, 5 × 600, and 1 × 480, and 1 × 960 s time frames. PET data were corrected for random coincidences, scatter and attenuation. During the scan, blood samples were drawn at 0, 5, 10, 15, 20, 30, 45, 60, 75, and 90 s and 2, 3, 5, 7, 10, 15, 30, 60, and 90 min after injection. Plasma samples taken at intervals of 2, 5, 10, 15, 30, 60 and 90 min were used for metabolite analysis using thin layer chromatography to determine two separate, average population-based metabolite curves for the control and pretreated animals. More information about animals, housing, anesthesia, surgery, PET imaging and blood sampling can be found in the supplemental materials.

Small-animal PET data analysis

Time activity curves for the striatum, midbrain, cerebellum and hippocampus were extracted from the dynamic PET data. Kinetic analysis was performed by fitting a 1TCM and 2TCM to the time activity curves using a blood and metabolite corrected plasma input function. Population average values were used as input function in two pretreated animals of ^{18}F-FPSCH where arterial blood sampling was not available. Besides the compartment models, a Logan graphical analysis of the PET data was performed with the linear fit starting at 9 min post injection. For both ^{18}F-FPSCH and ^{18}F-FESCH, V_T was determined for 1TCM and 2TCM and Logan graphical analysis whereas 1TCM and 2TCM fittings were compared using the AIC. More information about the PET data analysis can be found in the supplemental materials.

Once the most appropriate compartmental model was determined, hippocampus, midbrain and cerebellum were evaluated as reference region by calculating striatal DVR values relative to each of these regions. Since for the pretreated animals blocking was expected to be complete, DVR values shouldn't differ significantly from 1. For the control group, striatal DVR-1 values were compared to BP_{ND} using a SRTM for both a complete dynamic scan of 90 min and a dynamic scan of 60 min in order to assess the feasibility of reducing the acquisition time. We excluded cortical areas and brain regions close to the striatum as candidate reference regions, since such regions suffer from spill-over effects from the striatal specific binding and from the non-specific tracer uptake in the Harderian glands or in skull bone because of possible tracer defluorination.

RESULTS

^{18}F-FPSCH and ^{18}F-FESCH Distribution Volume

1TCM, 2TCM and Logan graphical analysis V_T data for ^{18}F-FPSCH and ^{18}F-FESCH in control and pretreated animals are presented in Table 2. The corresponding AIC values for 1TCM and 2TCM together with representative fits of both tracers are presented in Fig. 2. For ^{18}F-FPSCH, 2TCM AIC values proved to be lower than the 1TCM AIC values in 11 out of 48 cases, suggesting that 1TCM is most suitable model for ^{18}F-FPSCH. However, for ^{18}F-FESCH, 2TCM AIC values were lower than the corresponding 1TCM values in 35 out of 40 cases, suggesting that 2TCM is the most appropriate compartmental model for ^{18}F-FESCH.

^{18}F-FPSCH For the ^{18}F-FPSCH V_T values, a two way repeated measures analysis of variance (ANOVA) showed a significant interaction between brain region and model with Bonferroni posttests revealing significant differences in average striatal V_T values between 1TCM and the Logan plot while no significant differences between average 1TCM and 2TCM V_T values were found for all brain regions.

As 1TCM is the preferred compartmental model to describe ^{18}F-FPSCH tracer kinetics, 1TCM V_T values were further analyzed using a two way repeated measures ANOVA to determine the regional effect of pretreatment. This analysis showed a significant interaction between brain region and pretreatment, while Bonferroni posttests demonstrated a significant difference in average V_T values between control and pretreated animals for the striatum but not for hippocampus, midbrain and cerebellum.

For the pretreated animals, 1TCM DVR values representing the striatal ^{18}F-FPSCH uptake relative to the hippocampus, midbrain and cerebellum were respectively 1.10 ± 0.09, 1.04 ± 0.15 and 1.04 ± 0.11. These values were in all cases not significantly different from 1 (Wilcoxon Signed Rank Test, $p > 0.05$).

^{18}F-FESCH ^{18}F-FESCH V_T values were analyzed using a two way repeated measures ANOVA. This analysis showed a significant interaction between brain region and model with Bonferroni posttests revealing a significant difference in average V_T values between 1TCM and 2TCM for the hippocampus and cerebellum while no significant differences between average Logan and 2TCM V_T values were found for all brain regions.

Since 2TCM is the compartmental model of choice for ^{18}F-FESCH tracer kinetics, the effect of pretreatment on regional 2TCM V_T values was evaluated using a two way repeated measures ANOVA. This analysis showed a significant interaction between brain VOI and pretreatment with Bonferroni posttests demonstrating a significant difference in average V_T values between control and pretreated animals for the striatum but not for hippocampus, midbrain and cerebellum.

For the group of pretreated animals, 2TCM DVR values representing the striatal ^{18}F-FESCH uptake relative to the hippocampus, midbrain and cerebellum were respectively 1.13 ± 0.20, 1.16 ± 0.43 and 1.09 ± 0.44, i.e. not significantly different from 1 (Wilcoxon Signed Rank Test, $p > 0.05$).

^{18}F-FPSCH VS ^{18}F-FESCH Using a non-parametric, two-tailed Mann-Whitney test no significant differences were found between striatal ^{18}F-FESCH 2TCM V_T (5.0 ± 2.0) and striatal ^{18}F-FPSCH 1TCM V_T (3.7 ± 1.1) values in control animals ($p = 0.33$).

^{18}F-FPSCH and ^{18}F-FESCH Binding Potential

Striatal BP_{ND} values were calculated as 1TCM DVR–1 for ^{18}F-FPSCH and 2TCM DVR–1 for ^{18}F-FESCH and striatal BP_{ND} values for ^{18}F-FPSCH and ^{18}F-FESCH using SRTM and a 90 min and 60 min acquisition time interval. As reference region, hippocampus, midbrain and cerebellum were considered.

CONTROL GROUP SRTM BP_{ND} values for the control group are presented in Table 3. For this group, a one way repeated measures ANOVA (Friedman test) for each tracer and for each candidate reference region revealed no significant differences between striatal BP_{ND} values calculated as DVR–1 and striatal BP_{ND} values determined using SRTM and a 90 min or 60 min acquisition time interval except for the ^{18}F-FPSCH striatal BP_{ND} values using the midbrain as reference region. In that case, Dunn's multiple comparison post test showed a significant difference between striatal BP_{ND} calculated as 1TCM DVR–1 and SRTM BP_{ND} determined using a 60 min rather than a 90 min acquisition time interval.

Again for the control group, a Bland Altman comparison (% Difference) of ^{18}F-FPSCH striatal BP_{ND} values calculated as 1TCM DVR–1 with the striatal BP_{ND} values for ^{18}F-FPSCH using SRTM and a 90 min and 60 min acquisition time interval is presented in Table 4 for the three candidate reference regions. This is also presented for ^{18}F-FESCH in Table 5 where striatal BP_{ND} values calculated as 2TCM DVR–1 are compared with SRTM BP_{ND} values for a 90 min and 60 min acquisition time interval and for the different candidate reference regions. For visual assessment of the agreement between the different methods, striatal BP_{ND} values calculated as DVR–1 were also plotted in Fig. 3 against SRTM BP_{ND} values for a 90 min and 60 min acquisition time interval for both tracers and for the difference candidate reference regions.

PRETREATMENT GROUP For the pretreatment group, the BP_{ND} values of ^{18}F-FPSCH in the striatum using SRTM and 90 min or 60 min data acquisition were 0.11 ± 0.07 and 0.12 ± 0.07 (hippocampus as reference), 0.04 ± 0.12 and 0.05 ± 0.11 (midbrain as reference) and 0.04 ± 0.10 and 0.04 ± 0.11 (cerebellum as reference). The corresponding BP_{ND} values for ^{18}F-FESCH were 0.16 ± 0.21 and 0.21 ± 0.20, 0.14 ± 0.16 and 0.16 ± 0.15, and 0.04

± 0.28 and -0.02 ± 0.43, respectively. None of these values was significantly different from 0 (Wilcoxon Signed Rank Test, $p > 0.05$) except for the ^{18}F-FPSCH SRTM BP_{ND} values for a 90 min and 60 min acquisition time interval using the hippocampus as reference region.

^{18}F-FPSCH VS ^{18}F-FESCH Comparing striatal BP_{ND} values calculated as 1TCM DVR–1 for ^{18}F-FPSCH with striatal BP_{ND} values calculated as 2TCM DVR–1 values for the control group and for each candidate reference region using a non-parametric, two-tailed Mann-Whitney test, showed significant differences for the values calculated for the midbrain and cerebellum while no significant difference was observed for the hippocampus.

DISCUSSION

We evaluated two radiofluorinated analogs of SCH442416, ^{18}F-FPSCH and ^{18}F-FESCH, as ligands for PET imaging of $A_{2A}R$ expression in the rat brain. Based on AIC values, a 1TCM was the most appropriate model for describing ^{18}F-FPSCH kinetics while a 2TCM was the most suitable model for ^{18}F-FESCH kinetics. The evaluation of the different compartment models was limited to the tracer kinetics of the subcortical regions although previous studies with $A_{2A}R$ radioligands have used the centrum semiovale (*25*,*26*) and cerebral cortex as reference region (*27*,*28*). However, fitting of a two compartment model to tracer uptake in the cortical regions and cerebellum proved to be problematic for the dynamic ^{18}F-FPSCH scans. This was due to defluorination of the ^{18}F-FPSCH compound, resulting in accumulation of activity in the skull and bone structures surrounding the brain and confounding tracer kinetics of cortical regions and the cerebellum with an irreversible component. For this reason, the standard template based cerebellar brain VOI was adjusted manually to cover only the central part of the cerebellum such that these confounding spillover effects were minimized.

No significant differences were found between the striatal V_T values of both tracers in control animals, although the average V_T value in the striatum was higher for ^{18}F-FESCH (2TCM fit) than for ^{18}F-FPSCH (1TCM fit). For both tracers, striatal V_T values calculated from a Logan plot were lower than V_T values calculated from a compartment model fit, although this difference was only significant for ^{18}F-FPSCH. This observation is in line with literature data which report an underestimation of V_T by a Logan plot due to the impact of noise (*29*).

We observed a significant reduction of the striatal V_T values of both tracers after pretreatment. On the other hand, no significant decrease of tracer V_T values in hippocampus, midbrain and cerebellum was induced by the

pretreatment. Moreover, the striatal DVR relative to each of these three regions after pretreatment was not significantly different from 1, indicating that the non-displaceable tracer binding in the striatum is identical to the non-displaceable tracer binding in each of these three brain regions. These findings indicate that hippocampus, midbrain and cerebellum can be considered as suitable candidates for a reference tissue approach to quantify specific tracer binding in the striatum.

We evaluated SRTM for striatal BP_{ND} calculation in control animals using either hippocampus, midbrain or cerebellum as reference region and using a 60 min and 90 min dynamic PET scan. No significant differences were found between striatal SRTM BP_{ND} and DVR-1 values except for ^{18}F-FPSCH using a 60 min scanning interval and midbrain as reference region. For the pretreatment group, striatal SRTM BP_{ND} values for ^{18}F-FPSCH with the hippocampus as reference region differed significantly from zero while a value of zero was expected since full blocking of the $A_{2A}R$ was induced by pre dosing (*23*). Moreover for ^{18}F-FESCH, striatal SRTM BP_{ND} values with the hippocampus as reference region demonstrated a considerably higher coefficient of variation (Table 3) for the control group compared to SRTM BP_{ND} values using the other brain regions as reference tissue. Based on these findings, we conclude that midbrain and cerebellum are the reference regions of choice for SRTM BP_{ND} estimation of ^{18}F-FPSCH and ^{18}F-FESCH uptake in the rat brain. Selecting the cerebellum as a reference region for SRTM BP_{ND} quantification of the striatal uptake of an $A_{2A}R$ specific PET ligand is also supported by other PET studies (*15*,*19*,*20*,*30*).

A Bland Altman analysis comparing striatal SRTM BP_{ND} values with DVR–1 for ^{18}F-FPSCH (Table 4) and for ^{18}F-FESCH (Table 5) using both 90 min and 60 min dynamic PET data demonstrated that both brain regions perform similar in terms of bias and the 95 % confidence interval. The scanning time can be reduced to 60 min with a limited increase in bias and 95 % confidence interval. For a reduced scanning time of 60 min, cerebellum appeared to perform slightly better as a reference region for ^{18}F-FPSCH quantification while midbrain had the smallest bias and 95 % confidence interval for ^{18}F-FESCH quantification. This Bland Altman analysis also proves that SRTM provides accurate BP_{ND} values for specific striatal ^{18}F-FESCH uptake (Table 5) although 2TCM is the most appropriate compartment model for tracer ^{18}F-FESCH kinetics in both the striatum and candidate reference regions and SRTM assumes 1TCM tracer kinetics in both reference and target tissue. However, literature data have shown

that if the compartmental models of reference and target tissue are matched, the bias induced by SRTM is minimal (*31*,*32*).

Other $A_{2A}R$ specific PET ligands that have been developed are ^{18}F-MNI-444, ^{11}C-TMSX, ^{11}C-KW-6002, ^{11}C-SCH442416 and ^{11}C-preladenant (*16*,*23-26*,*28*,*30*,*33*). Except for ^{18}F-MNI-444 and ^{11}C-preladenant, $A_{2A}R$ quantification using these tracers is challenging, because of the low specific to non-specific binding ratio or high extra-striatal binding. ^{18}F-MNI-444 was tested in the rhesus monkeys and human subjects, demonstrating good brain penetration with BP_{ND} values ranging from 2.6 to 4.9 in $A_{2A}R$-rich regions (*15*,*16*). On the other hand, ^{11}C-preladenant has striatal BP_{ND} values around 5.5 and fast tracer kinetics such that a 60 min acquisition time is sufficient for accurate $A_{2A}R$ quantification in a rat brain. However, ^{11}C-labeled PET tracers have some intrinsic disadvantages due to the short half-life. On the other hand, ^{18}F-FPSCH and ^{18}F-FESCH are fluorinated compounds, therefore providing more flexibility in terms of imaging, and demonstrated similar tracer kinetics as ^{11}C-preladenant with BP_{ND} values around 2.5. Comparing ^{18}F-FPSCH and ^{18}F-FESCH, striatal SRTM BP_{ND} values using either midbrain or cerebellum as reference region proved to be significantly lower for ^{18}F-FPSCH compared to ^{18}F-FESCH. Taking into account this finding and the Bland Altman analysis demonstrating the smaller bias for ^{18}F-FESCH compared to ^{18}F-FPSCH for a 60 min scan duration, ^{18}F-FESCH is preferred over ^{18}F-FPSCH for PET imaging of $A_{2A}R$ expression in the rat brain. However, for translation into a clinical setting, the presented metabolite results and optimal compartmental models need to be re-evaluated for ^{18}F-FESCH brain uptake in humans, because of possible interspecies differences in tracer kinetics and metabolism. Since the cerebellum demonstrated low to negligible $A_{2A}R$ density in autoradiography experiments with human brain tissue (*34*), previous studies with $A_{2A}R$-specific radiotracers in humans have used the cerebellum as a reference region (*16*). This reference tissue approach could also be considered for the quantification of ^{18}F-FESCH in a clinical setting, thus avoiding the need for arterial sampling and metabolite analysis.

CONCLUSION

We evaluated two radio-fluorinated analogs of SCH442416, ^{18}F-FPSCH and ^{18}F-FESCH, as PET ligands for imaging $A_{2A}R$ expression in a rat brain. Full kinetic analysis using arterial blood sampling indicated 1TCM and 2TCM as the most suitable model for ^{18}F-FPSCH and ^{18}F-FESCH respectively. Dynamic PET imaging under baseline and full blocking conditions determined ^{18}F-FESCH as the most suitable PET ligand for quantifying $A_{2A}R$

expression in the rat brain. Accurate quantification of the striatal specific binding is achieved by a 60 min dynamic PET scan and SRTM with either cerebellum or midbrain as reference region.

ACKNOWLEDGMENTS

We thank Jurgen Sijbesma, MA Khayum and Soumen Paul for their technical assistance.

REFERENCES

1. Fredholm BB, Abbracchio MP, Burnstock G, et al. Nomenclature and classification of purinoceptors. *Pharmacol Rev.* 1994;46:143-156.

2. Hess S. Recent advances in adenosine receptor antagonist research. *Expert Opin Ther Pat.* 2001;11:1533-1561.

3. Ishiwata K, Kimura Y, de Vries EFJ, Elsinga PH. PET Tracers for mapping adenosine receptors as probes for diagnosis of CNS disorders. *Cent Nerv Syst Agents Med Chem.* 2007;7:57-77.

4. Palmer TM, Stiles GL. Adenosine receptors. *Neuropharmacology.* 1995;34:683-694.

5. Jacobson KA. Introduction to adenosine receptors as therapeutic targets. *Handb Exp Pharmacol.* 2009;193:1-24.

6. Khanapur S, Paul S, Shah A, et al. Development of [18F]-labeled pyrazolo[4,3-e]-1,2,4- triazolo[1,5-c]pyrimidine (SCH442416) analogs for the imaging of cerebral adenosine A2A receptors with positron emission tomography. *J Med Chem.* 2014;57:6765-6780.

7. Fastbom J, Pazos A, Palacios JM. The distribution of adenosine A1 receptors and 5'-nucleotidase in the brain of some commonly used experimental animals. *Neuroscience.* 1987;22:813-826.

8. Martinez-Mir MI, Probst A, Palacios JM. Adenosine A2 receptors: selective localization in the human basal ganglia and alterations with disease. *Neuroscience.* 1991;42:697-706.

9. Ji XD, Stiles GL, van Galen PJ, Jacobson KA. Characterization of human striatal A2-adenosine receptors using radioligand binding and photoaffinity labeling. *J Recept Res.* 1992;12:149-169.

10. Parkinson FE, Fredholm BB. Autoradiographic evidence for G-protein coupled A2-receptors in rat neostriatum using [3H]-CGS 21680 as a ligand. *Naunyn Schmiedebergs Arch Pharmacol.* 1990;342:85-89.

11. Tavares AA, Batis JC, Papin C, et al. Kinetic modeling, test-retest, and dosimetry of 123I-MNI-420 in humans. *J Nucl Med.* 2013;54:1760-1767.

12. Schiffmann SN, Fisone G, Moresco R, Cunha RA, Ferre S. Adenosine A2A receptors and basal ganglia physiology. *Prog Neurobiol.* 2007;83:277-292.

13. Schwarzschild MA, Agnati L, Fuxe K, Chen JF, Morelli M. Targeting adenosine A2A receptors in Parkinson's disease. *Trends Neurosci.* 2006;29:647-654.

14. Ferre S, Quiroz C, Orru M, et al. Adenosine A(2A) Receptors and A(2A) Receptor Heteromers as Key Players in Striatal Function. *Front Neuroanat.* 2011;5:36.

15. Barret O, Hannestad J, Alagille D, et al. Adenosine 2A receptor occupancy by tozadenant and preladenant in rhesus monkeys. *J Nucl Med.* 2014;55:1712-1718.

16. Barret O, Hannestad J, Vala C, et al. Characterization in humans of 18F-MNI-444, a PET radiotracer for brain adenosine 2A receptors. *J Nucl Med.* 2015;56:586-591.

17. Bhattacharjee AK, Lang L, Jacobson O, et al. Striatal adenosine A(2A) receptor mediated PET Imaging in 6-hydroxydopamine lesioned rats using [(18)F]-MRS5425. *Nucl Med Biol.* 2011;38:897-906.

18. Hirani E, Gillies J, Karasawa A, et al. Evaluation of [4-O-methyl-(11)C]KW-6002 as a potential PET ligand for mapping central adenosine A(2A) receptors in rats. *Synapse.* 2001;42:164-176.

19. Ishiwata K, Noguchi J, Wakabayashi S, et al. 11C-labeled KF18446: a potential central nervous system adenosine A2a receptor ligand. *J Nucl Med.* 2000;41:345-354.

20. Moresco RM, Todde S, Belloli S, et al. In vivo imaging of adenosine A2A receptors in rat and primate brain using [11C]SCH442416. *Eur J Nucl Med Mol Imaging.* 2005;32:405-413.

21. Noguchi J, Ishiwata K, Wakabayashi S, et al. Evaluation of carbon-11-labeled KF17837: a potential CNS adenosine A2a receptor ligand. *J Nucl Med.* 1998;39:498-503.

22. Stone-Elander S, Thorell JO, Eriksson L, Fredholm BB, Ingvar M. In vivo biodistribution of [N-11C-methyl]KF 17837 using 3-D-PET: evaluation as a ligand for the study of adenosine A2A receptors. *Nucl Med Biol.* 1997;24:187-191.

23. Zhou X, Khanapur S, de Jong JR, et al. In vivo evaluation of [11C]preladenant positron emission tomography for quantification of adenosine A2A receptors in the rat brain. *J Cereb Blood Flow Metab.* 2016.

24. Brooks DJ, Doder M, Osman S, et al. Positron emission tomography analysis of [11C]KW-6002 binding to human and rat adenosine A2A receptors in the brain. *Synapse.* 2008;62:671-681.

25. Naganawa M, Kimura Y, Mishina M, et al. Quantification of adenosine A2A receptors in the human brain using [11C]TMSX and positron emission tomography. *Eur J Nucl Med Mol Imaging.* 2007;34:679-687.

26. Mishina M, Ishiwata K, Kimura Y, et al. Evaluation of distribution of adenosine A2A receptors in normal human brain measured with [11C]TMSX PET. *Synapse.* 2007;61:778-784.

27. Mishina M, Kimura Y, Naganawa M, et al. Differential effects of age on human striatal adenosine A(1) and A(2A) receptors. *Synapse.* 2012;66:832-839.

28. Mishina M, Ishiwata K, Naganawa M, et al. Adenosine A(2A) receptors measured with [C]TMSX PET in the striata of Parkinson's disease patients. *PLoS One.* 2011;6:e17338.

29. Slifstein M, Laruelle M. Effects of statistical noise on graphic analysis of PET neuroreceptor studies. *J Nucl Med.* 2000;41:2083-2088.

30. Ramlackhansingh AF, Bose SK, Ahmed I, Turkheimer FE, Pavese N, Brooks DJ. Adenosine 2A receptor availability in dyskinetic and nondyskinetic patients with Parkinson disease. *Neurology.* 2011;76:1811-1816.

31. Slifstein M, Parsey RV, Laruelle M. Derivation of [(11)C]WAY-100635 binding parameters with reference tissue models: effect of violations of model assumptions. *Nucl Med Biol.* 2000;27:487-492.

32. Salinas CA, Searle GE, Gunn RN. The simplified reference tissue model: model assumption violations and their impact on binding potential. *J Cereb Blood Flow Metab.* 2015;35:304-311.

33. Naganawa M, Mishina M, Sakata M, et al. Test-retest variability of adenosine A2A binding in the human brain with (11)C-TMSX and PET. *EJNMMI Res.* 2014;4:76.

34. Svenningsson P, Hall H, Sedvall G, Fredholm BB. Distribution of adenosine receptors in the postmortem human brain: an extended autoradiographic study. *Synapse.* 1997;27:322-335.

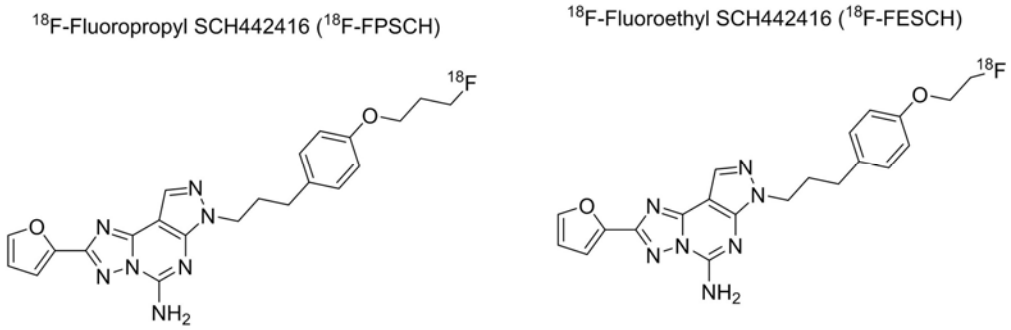

FIGURE 1. Chemical structures of ^{18}F-labeled SCH442416 analogs.

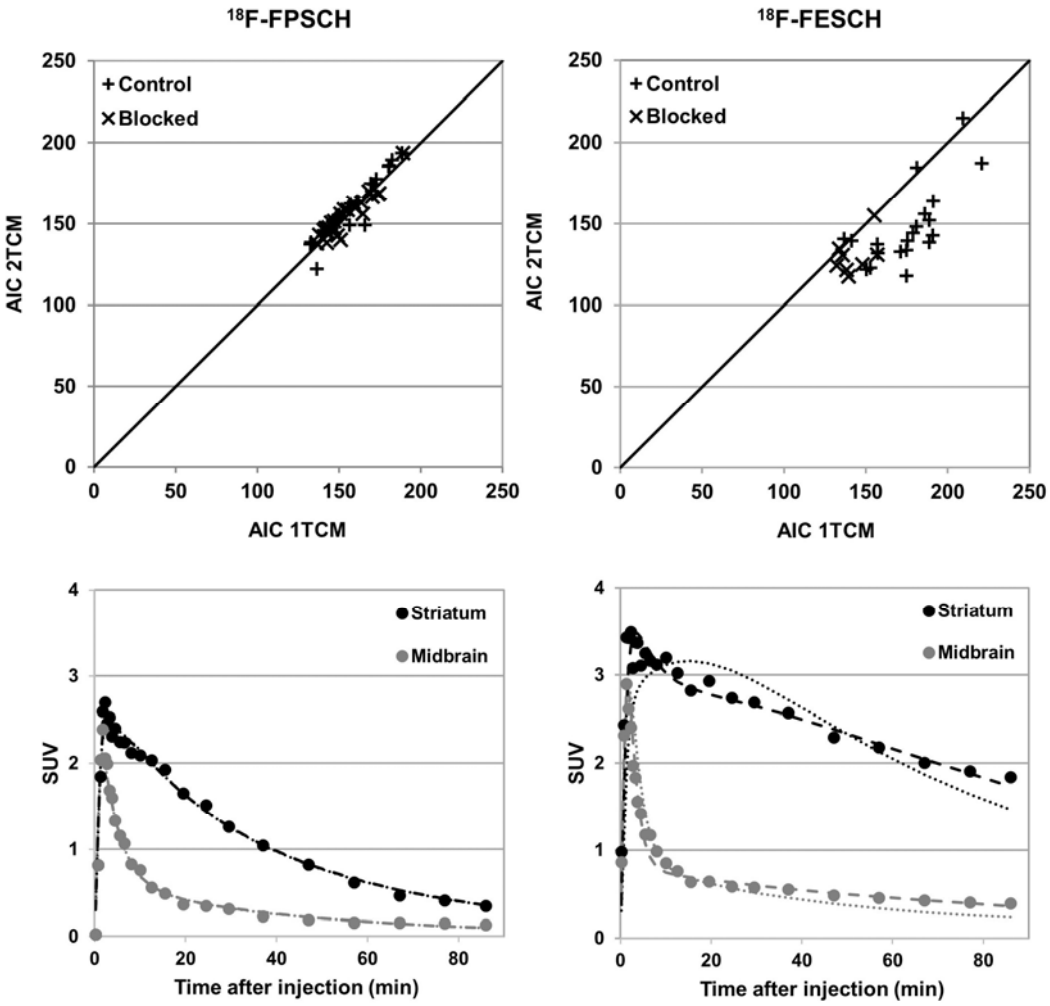

FIGURE 2. AIC values for 1TCM and 2TCM (upper row) and a representative 1TCM (dotted line) and 2TCM (dashed line) fitting (lower row) for both ^{18}F-FPSCH and ^{18}F-FESCH.

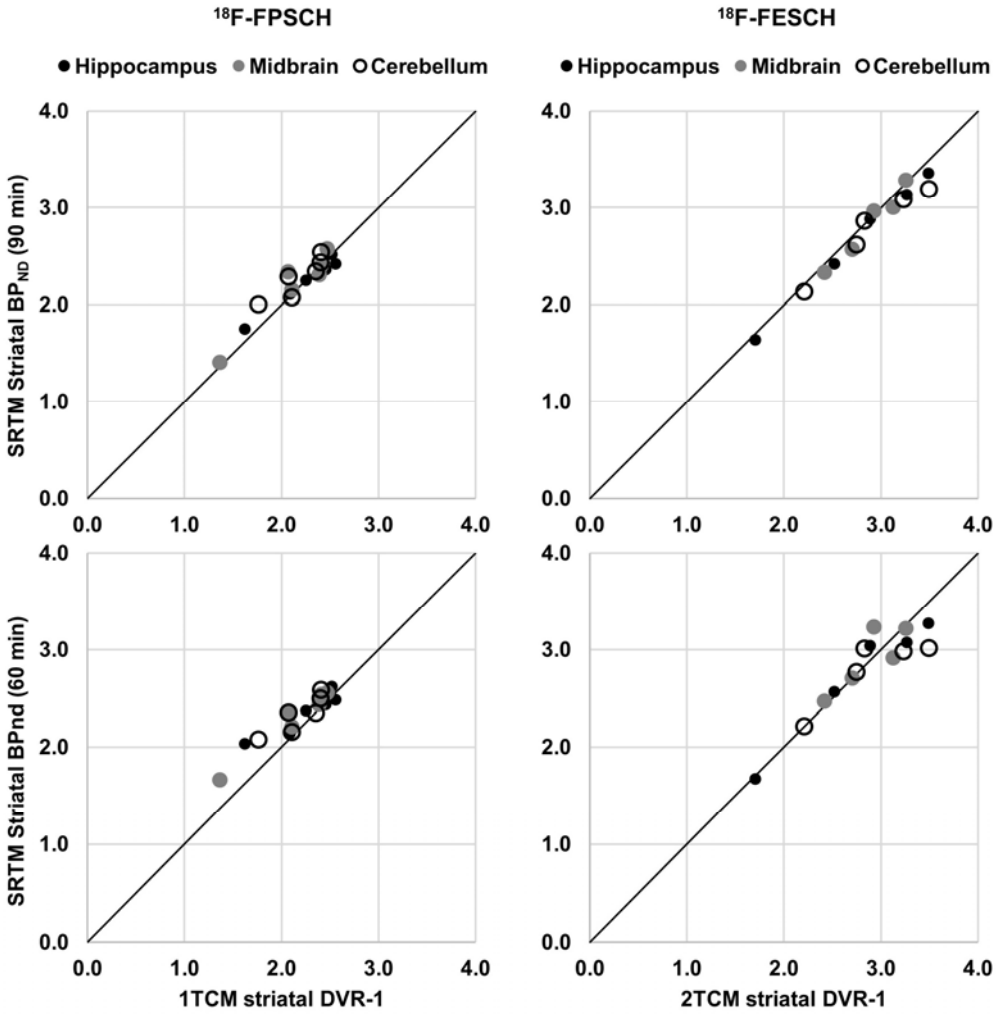

FIGURE 3. Graphical overview of the striatal BP_{ND} values calculated as DVR–1 and using SRTM with a 90 min and 60 min scan duration.

	^{18}F-FPSCH		^{18}F-FESCH	
Group (# male Wistar rats)	Vehicle-control (n = 6)	Pretreated (n = 6)	Vehicle-control (n = 5)	Pretreated (n = 5)
Body weight (g)	295 ± 19	293 ± 31	312 ± 14	321 ± 15
Injected mass dose (nM)	0.21 ± 0.11	0.29 ± 0.27	1.13 ± 0.41	0.74 ± 0.62

TABLE 1. Vehicle-control and pretreated group for dynamic PET scanning of a rat brain with ^{18}F-FPSCH and ^{18}F-FESCH. Pretreatment was done with KW-6002 ($A_{2A}R$ antagonist, 1 mg / kg). Data are presented as mean ± SD.

		^{18}F-FPSCH			^{18}F-FESCH		
		1TCM	**2TCM**	**LGA**	**1TCM**	**2TCM**	**LGA**
STR	**CTR**	3.69±1.11 (30.00%)	3.72±1.10 (29.53%)	3.52±1.11 (31.62%)	4.80±1.69 (35.21%)	5.00±1.96 (39.13%)	4.66±1.95 (41.96%)
	PTR	0.98±0.38 (38.14%)	1.00±0.39 (38.70%)	0.96±0.32 (33.46%)	1.00±0.28 (28.18%)	1.22±0.26 (21.71%)	1.19±0.20 (17.03%)
HC	**CTR**	1.13±0.29 (25.54%)	1.14±0.32 (27.92%)	1.13±0.26 (22.89%)	1.16±0.21 (18.40%)	1.29±0.29 (22.72%)	1.25±0.30 (24.20%)
	PTR	0.90±0.35 (39.41%)	0.91±0.37 (40.73%)	0.98±0.35 (35.37%)	0.75±0.19 (25.03%)	1.10±0.28 (25.56%)	1.00±0.20 (19.66%)
MB	**CTR**	1.16±0.27 (22.96%)	1.17±0.26 (22.34%)	1.15±0.23 (20.39%)	1.15±0.29 (25.13%)	1.26±0.40 (31.43%)	1.22±0.37 (30.26%)
	PTR	0.97±0.39 (40.16%)	0.99±0.40 (40.44%)	1.07±0.49 (45.45%)	0.83±0.15 (17.78%)	1.18±0.41 (34.63%)	1.05±0.15 (14.63%)
CB	**CTR**	1.15±0.29 (25.63%)	1.14±0.29 (25.31%)	1.07±0.29 (26.69%)	1.14±0.27 (23.79%)	1.25±0.34 (27.50%)	1.22±0.35 (28.67%)
	PTR	0.95±0.37 (38.85%)	0.97±0.39 (39.90%)	0.96±0.32 (33.44%)	0.82±0.13 (15.62%)	1.40±0.49 (35.11%)	1.14±0.13 (11.47%)

TABLE 2. ^{18}F-FPSCH and ^{18}F-FESCH V_T values using 1TCM, 2TCM and Logan graphical analysis (LGA) for both the control (CTR) and pretreatment (PTR) group and for the striatum (STR), Hippocampus (HC), Midbrain (MB) and Cerebellum (CB). Data are presented as mean ± SD (CoV).

	^{18}F-FPSCH			^{18}F-FESCH		
	1TCM (DVR-1)	**SRTM (90 min)**	**SRTM (60 min)**	**2TCM (DVR-1)**	**SRTM (90 min)**	**SRTM (60 min)**
Hippocampus	2.25±0.35 (15.77%)	2.23±0.27 (12.29%)	2.35±0.22 (9.40%)	2.78±0.70 (25.30%)	2.69±0.68 (25.33%)	2.72±0.64 (23.65%)
Midbrain	2.14±0.41 (19.28%)	2.19±0.41 (18.63%)	2.29±0.33 (14.56%)	2.89±0.34 (11.60%)	2.83±0.38 (13.38%)	2.91±0.33 (11.38%)
Cerebellum	2.19±0.25 (11.64%)	2.28±0.21 (9.09%)	2.33±0.20 (8.83%)	2.91±0.49 (16.94%)	2.78±0.42 (15.24%)	2.80±0.34 (12.28%)

TABLE 3. Baseline striatal BP_{ND} values calculated as DVR–1 and using SRTM with a 90 min and 60 min scan duration. Hippocampus, midbrain and cerebellum were considered as reference region. Data are presented as mean ± SD (CoV).

	SRTM (90 min)			SRTM (60 min)		
	Hippocampus	**Midbrain**	**Cerebellum**	**Hippocampus**	**Midbrain**	**Cerebellum**
Bias (%)	-0.4	2.8	4.4	4.9	7.8	6.9
SD of bias (%)	4.6	5.2	5.8	9.0	6.8	6.4
95% limits of agreement (%)	[-9.4,8.6]	[-7.5,13.0]	[-7.1,15.8]	[-12.8,22.5]	[-5.6,21.2]	[-5.7,19.4]

TABLE 4. Bland Altman comparison of striatal BP_{ND} calculated as 1TCM DVR–1 and using SRTM for baseline ^{18}F-FPSCH PET with a 90 min and 60 min scan duration. Hippocampus, Midbrain and Cerebellum were considered as reference region. % Difference vs average was calculated.

	SRTM (90 min)			SRTM (60 min)		
	Hippocampus	**Midbrain**	**Cerebellum**	**Hippocampus**	**Midbrain**	**Cerebellum**
Bias (%)	-3.3	-2.3	-4.4	-1.7	0.6	-3.3
SD of bias (%)	1.7	3.0	3.7	5.0	6.1	8.2
95% limits of agreement (%)	[-6.6,-0.1]	[-8.1,3.5]	[-11.5,2.8]	[-11.4,8.1]	[-11.4,12.6]	[-19.4, 12.7]

TABLE 5. Bland Altman comparison of striatal BP_{ND} calculated as 2TCM DVR–1 and using SRTM for baseline ^{18}F-FESCH PET with a 90 min and 60 min scan duration. Hippocampus, Midbrain and Cerebellum were considered as reference region. % Difference vs average was calculated.

Supplemental Materials:

Preclinical Evaluation and Quantification of ^{18}F-Fluoroethyl and ^{18}F-Fluoropropyl analogs of SCH442416 as Radioligands for PET Imaging of the Adenosine A_{2A} Receptors in Rat Brain

Shivashankar Khanapur[1], Aren van Waarde[1], Rudi A.J.O. Dierckx[1], Philip H. Elsinga[1], Michel J.B. Koole[1,2]

[1]Department of Nuclear Medicine and Molecular Imaging, University of Groningen, University Medical Center Groningen, Groningen, The Netherlands

[2]Department of Nuclear Medicine and Molecular Imaging, KU Leuven, Leuven, Belgium

MATERIALS AND METHODS

General

The compounds SCH442416 and KW-6002 were purchased from Axon Medchem BV (Groningen, The Netherlands). 1,2-Ethanediol di-p-tosylate and 1,3-Propanediol di-p-tosylate were acquired from Aldrich (Sigma-Aldrich, The Netherlands). All other chemicals were of analytical grade and were obtained from commercial suppliers such as Fluka, Rathburn, Sigma and Merck, and were used without further purification.

Radiosynthesis of ^{18}F-FESCH and ^{18}F-FPSCH

In brief, tracers were prepared by a two-step two-pot radiosynthetic method, starting with the corresponding intermediate ^{18}F-fluorosynthons (2-^{18}F-fluoroethyltosylate and 3-^{18}F-fluoropropyltosylate), followed by selective fluoroalkylation of the O-desmethyl precursor.

Small-animal PET scanning

Male outbred Wistar-Unilever rats were obtained from Harlan (The Netherlands). The animals were housed in Macrolon polycarbonate breeding cages (38 × 26 × 24 cm), maintained at a 12-h light / 12-h dark regime and were fed standard laboratory chow (RMH-B, The Netherlands) and water *ad libitum*. After arrival, the rats were allowed to acclimatize for at least seven days. During PET imaging, all animals were anesthetized with isoflurane/medical air (inhalation anesthesia, 5 % during induction, $\leqslant$ 2 % during maintenance) and were kept on electronic heating pads during the entire study period. Both a femoral artery and a femoral vein were cannulated for blood sampling and tracer injection, respectively. A Harvard-style syringe pump at a speed of 1mL / min was used for tracer injection. In addition, oxygen saturation and heart rate were measured using a pulse

oximeter (Nonin, The Netherlands) with an optical sensor attached to the hind leg. These parameters were maintained within physiological limits by manual adjustment of the anesthesia parameters (isoflurane concentration, gas flow). In each scan session, two rats were scanned simultaneously (supine position) using a Focus 220 microPET camera (CTI, Siemens, Germany). The brains of both rats were placed in the field of view. Before the emission scan, a transmission scan of 515 s was performed using a ^{57}Co point source. The emission scan was acquired in list mode for 106 min, starting at the moment the tracer entered the body of the first rat; the second animal was injected 16 min later. Dynamic PET data were acquired in list-mode and rebinned into 8 × 30, 3 × 60, 2 × 120, 2 × 180, 3 × 300, 5 × 600, and 1 × 480, and 1 × 960s time frames with one rebinning starting at the injection time of the first animal while the second rebinning took into account the delayed injection of the second animal. Time frames were reconstructed using a 2D ordered subsets expectation maximization algorithm (4 iterations, 16 subsets, Zoom factor, 2). The reconstructed images were smoothed with a 3D Gaussian filter (1.35 mm full width at half-maximum in both directions) and split so that a separate dataset was available for each animal with the proper timings. During the dynamic PET scan, blood samples (volume 0.1-0.15 mL) were taken from the cannulation of the femoral artery. After collecting 25µL of whole blood, plasma (25 µL) was acquired from the remainder of the blood samples by short centrifugation (5 min at 1000 *g*). Radioactivity in both 25 µL plasma and whole blood was counted on a γ-counter (CompuGamma 1282 CS, LKB-Wallac, Turku, Finland).

Small-animal PET data analysis

PET data analysis was performed using Inveon Research Workplace (Siemens Medical Solutions, Knoxville, TN). The summed PET time frames from each animal were co-registered to an MRI template of a rat brain with predefined volumes of interest. Translation, rotation and scaling were adjusted to visually optimize the fusion of the images. Volumes of interest were transferred from the MRI template to the PET data, and tissue time activity curves were extracted and rescaled to

standardized uptake values using measured body weight and injected dose. Compartmental models were fitted to the time activity curves using a blood and metabolite-corrected data from arterial plasma samples and uncorrected data from whole blood samples as input functions while cerebral blood volume was fixed to 0.036 (*1*). A single exponential was fitted to the parent fraction data while a triple exponential was fitted to the whole blood and plasma radioactivity data. PET frames were weighted according to the frame duration and frame mid time relative to the start of the acquisition. A delay parameter describing a timing offset between tissue and blood data was fitted simultaneously with the compartment model.

REFERENCES

1. Julien-Dolbec C, Tropres I, Montigon O, et al. Regional response of cerebral blood volume to graded hypoxic hypoxia in rat brain. *Br J Anaesth.* 2002;89:287-293.

The Journal of NUCLEAR MEDICINE

Preclinical Evaluation and Quantification of ^{18}F-Fluoroethyl and ^{18}F-Fluoropropyl analogs of SCH442416 as Radioligands for PET Imaging of the Adenosine A $_{2A}$ Receptors in Rat Brain

Shivashankar Khanapur, Aren van Waarde, Rudi A. Dierckx, Philip H Elsinga and Michel Koole

J Nucl Med.
Published online: October 27, 2016.
Doi: 10.2967/jnumed.116.178103

The Journal of Nuclear Medicine is published monthly.
SNMMI | Society of Nuclear Medicine and Molecular Imaging
1850 Samuel Morse Drive, Reston, VA 20190.
(Print ISSN: 0161-5505, Online ISSN: 2159-662X)

SNMMI SOCIETY OF NUCLEAR MEDICINE AND MOLECULAR IMAGING